Journal of Magnetic Resonance **143,** 407–410 (2000)
doi:10.1006/jmre.2000.2030, available online at http://www.idealibrary.com on IDEAL®

Sensitivity Enhancement of HCACO by Using an HMQC Magnetization Transfer Scheme

Youlin Xia,*,† Xiangming Kong,* David K. Smith,‡ Yu Liu,* David Man,* and Guang Zhu*,[1]

*Department of Biochemistry, The Hong Kong University of Science and Technology, Clear Water Bay, Kowloon, Hong Kong; †School of Life Science, University of Science and Technology of China, Hefei, People's Republic of China; and ‡Department of Biochemistry, The University of Hong Kong, Pok Fu Lam, Hong Kong

Received July 30, 1999; revised January 12, 2000

Previous theoretical calculations have demonstrated that the multiquantum relaxation rate of $^1H^\alpha$–$^{13}C^\alpha$(R_{MQ}) is, on average, 1.3 ± 0.4 or 1.7 ± 0.6 times slower than the single-quantum relaxation rate of $^{13}C^\alpha$(R_C) for a sample with or without, respectively, amide protons. By taking advantage of this fact and by using the PEP sensitivity enhancement scheme, an HMQC version of the HCACO experiment has been developed. We demonstrate that this new experiment is 23 and 55% more sensitive than the original HSQC version of the HCACO experiment, at constant times of 7 and 27 ms, respectively, for a sample of the BC domain of the ciliary neurotrophic factor receptor protein dissolved in D_2O at 20°C. © 2000 Academic Press

Key Words: **NMR; ^{13}C-labeled proteins; HCACO; HMQC.**

Many 3D NMR experiments have been developed to assist the resonance assignment of isotopically labeled proteins. One useful experiment for backbone chemical shift assignment, which correlates the chemical shifts of the intraresidue $^1H^\alpha$, $^{13}C^\alpha$, and $^{13}C'$ resonances, is the HSQC-based 3D HCACO (HSQC-HCACO) experiment. Since its inception (*1*), the HCACO experiment has been modified several times to increase its sensitivity and resolution (*2–6*). In this report, we demonstrate that the sensitivity of this experiment can be further improved, as the relaxation time of $^1H^\alpha$–$^{13}C^\alpha$ multiquantum coherence is longer than that of single-quantum coherence. Theoretical calculations have shown that the multiquantum relaxation rate of $^1H^\alpha$–$^{13}C^\alpha$(R_{MQ}) is, on average, 1.3 ± 0.4 or 1.7 ± 0.6 times slower than the single-quantum relaxation rate of $^{13}C^\alpha$(R_C) for a sample with or without, respectively, amide protons (*7, 8*).

The improved experiment described here employs the HMQC sensitivity enhancement scheme, developed earlier (*7–10*), to increase sensitivity. For HMQC-HCACO experiments with constant time periods ($2T_C$) of 7 and 27 ms, sensitivities increased, on average, by 23 and 55%, respectively, when compared with the corresponding HSQC-HCACO experiments on the 11-kDa BC domain of the ciliary neurotrophic factor receptor (CNTFR) dissolved in D_2O at 20°C. In addition, this experiment removes $^{13}C^\alpha$–$^{13}C^\beta$ homonuclear *J* couplings (*4*) and so allows prompt assignment of the glycine cross peaks, as they have opposite signs to all other C^α correlations when $2T_C$ is set to 27 ms, due to $^{13}C^\alpha$ of Gly not being coupled to an aliphatic carbon.

Figure 1 depicts the pulse sequence of the constant-time HCACO experiment based on the HMQC magnetization transfer scheme. In the HMQC-HCACO pulse sequence, the section before point a creates the multiple-quantum coherence of $^1H^\alpha$ and $^{13}C^\alpha$. During the following period of $2\tau_1$ the magnetization of $^{13}C^\alpha$ is transferred to $^{13}C'$, while the transverse magnetization of $^1H^\alpha$ is locked along the *x*-axis, so that homonuclear couplings between $^1H^\alpha$ and other protons are removed. However, the strength of spin-lock field must not be too high in order to avoid homonuclear Hartmann–Hahn effects. Hence, for protons whose resonance frequencies are far from the carrier of the spin-lock RF field, the transverse magnetization cannot be locked effectively, and their signal intensities decrease. The transverse coherence is labeled with the $^{13}C'$ frequency during the t_1 period. In the section between points c and d, $^{13}C^\alpha$ magnetization evolves in a constant-time manner, the anti-phase magnetization of $^{13}C^\alpha$ with respect to $^{13}C'$ is refocused, and the transverse magnetization of $^1H^\alpha$ is locked along the *x*-axis for the reason given above. If $2T_C = 27$ ms, the signal is not reduced during the constant-time period by the coupling of $^{13}C^\alpha$ and $^{13}C^\beta$, because $\cos(2\pi J_{C\alpha C\beta} T_C) \approx 1$. Finally, between points d and e, the two transverse magnetization components of $^{13}C^\alpha$ are transferred to $^1H^\alpha$ through the PEP (preservation of equivalent path) method (*11–15*), before detection. For nonglycine residues, the use of PEP results in an increase in sensitivity by a factor of 1.36 (*9–15*); however the sensitivities of glycine residues are reduced by about 50%.

The evolution of the magnetization at different time points is given as

[1] To whom correspondence should be addressed. Fax: 852-2358-1552. E-mail: gzhu@ust.hk.

1090-7807/00 $35.00

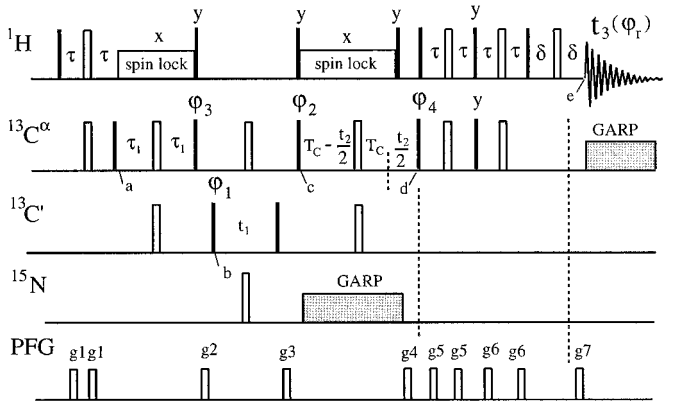

FIG. 1. HMQC version of the HCACO pulse sequence. In the pulse sequence, filled bars and open bars represent 90° and 180° pulses, respectively. Default phases are x. The carriers of ^{1}H, $^{13}C^\alpha$, $^{13}C'$, and ^{15}N are set at 4.7, 56, 176, and 120 ppm, respectively. Phase cycling is as follows: $\varphi_1 = (x, x, -x, -x)$; $\varphi_2 = (x, -x)$; $\varphi_3 = (y, y, y, y, -y, -y, -y, -y)$; $\varphi_4 = (x)$; $\varphi_r = (x, -x, -x, x, -x, x, x, -x)$. Quadrature components in t_1 are acquired through altering φ_1 in a States–TPPI manner. Echo/anti-echo selections during t_2 are performed by setting $\varphi_4 = (-x)$ and inverting the sign of g4. Axial peaks in the F2 dimension are removed by setting (φ_2 + 180°, φ_r + 180°) for every second t_2. The experimental recovery delay is 1 s; $2\tau = 1/(2\,^1J_{CH}) \approx 3.4$ ms; $2\tau_1 = 7.0$ ms; and $2T_C = 7$ ms or 27 ms. δ is set to the corresponding gradient pulse width plus a gradient recovery time of 90 μs. The duration and strength of the gradients are set to g1 = (0.4 ms, 5 G/cm); g2 = (0.4 ms, 15 G/cm); g3 = (0.4 ms, 10 G/cm); g4 = (1.0 ms, −25 G/cm); g5 = (0.5 ms, 5 G/cm); g6 = (0.4 ms, 5 G/cm); g7 = (0.25 ms, 25 G/cm). The power of the spin lock is 5 kHz and the carrier of the spin-lock field is set at 4.1 ppm.

$$\sigma_a = 2H_x^\alpha C_y^\alpha,$$

$$\sigma_b = -4\,\sin(2\pi J_{C\alpha C'}\tau_1)\cos(2\pi J_{C\alpha C\beta}\tau_1)H_z^\alpha C_z^\alpha C_y',$$

$$\sigma_c = 4\,\sin(2\pi J_{C\alpha C'}\tau_1)\cos(2\pi J_{C\alpha C\beta}\tau_1) \times \cos(\Omega_{C'}t_1)H_x^\alpha C_y^\alpha C_z',$$

$$\sigma_d = 2\,\sin(2\pi J_{C\alpha C'}\tau_1)\cos(2\pi J_{C\alpha C\beta}\tau_1) \times \sin(2\pi J_{C\alpha C'}T_c)\cos(2\pi J_{C\alpha C\beta}T_c) \times \cos(\Omega_{C'}t_1)H_z^\alpha[C_y^\alpha\cos(\Omega_{C\alpha}t_2) - C_x^\alpha\sin(\Omega_{C\alpha}t_2)],$$

$$\sigma_e = \sin(2\pi J_{C\alpha C'}\tau_1)\cos(2\pi J_{C\alpha C\beta}\tau_1) \times \sin(2\pi J_{C\alpha C'}T_c)\cos(2\pi J_{C\alpha C\beta}T_c) \times \cos(\Omega_{C'}t_1)[H_y^\alpha\cos(\Omega_{C\alpha}t_2 + \Omega_{H\alpha}t_3) - H_x^\alpha\sin(\Omega_{C\alpha}t_2 + \Omega_{H\alpha}t_3)],$$

Where H^α, C^α, and C' are the spin operators of $^1H^\alpha$, $^{13}C^\alpha$, and $^{13}C'$, respectively, J_{xy} is the single-bond coupling constant of spins x and y, and Ω_x is the chemical shift of spin x. The four transients recorded for every pair of t_1 and t_2 can be expressed as

$$S_{11} \propto S_0\cos(\Omega_{C'}t_1)\exp(+i\Omega_{C\alpha}t_2)\exp(i\Omega_{H\alpha}t_3)$$

$$S_{12} \propto S_0\cos(\Omega_{C'}t_1)\exp(-i\Omega_{C\alpha}t_2)\exp(i\Omega_{H\alpha}t_3)$$

$$S_{21} \propto S_0\sin(\Omega_{C'}t_1)\exp(+i\Omega_{C\alpha}t_2)\exp(i\Omega_{H\alpha}t_3)$$

$$S_{22} \propto S_0\sin(\Omega_{C'}t_1)\exp(-i\Omega_{C\alpha}t_2)\exp(i\Omega_{H\alpha}t_3),$$

with S_0 being defined as

$$S_0 = \sin(2\pi J_{C\alpha C'}\tau_1)\cos(2\pi J_{C\alpha C\beta}\tau_1) \times \sin(2\pi J_{C\alpha C'}T_c)\cos(2\pi J_{C\alpha C\beta}T_c).$$

The real part of the FID for t_2 can be obtained by adding S_{11} to S_{12} and S_{21} to S_{22}. The corresponding imaginary part of the

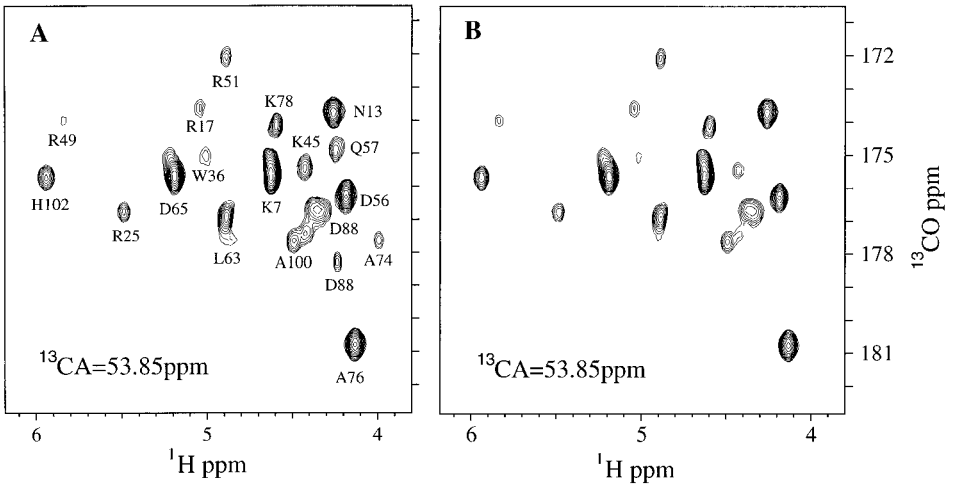

FIG. 2. 2D spectral slices taken from the 3D HMQC-HCACO spectrum (A) and its corresponding 3D HSQC-HCACO spectrum (B) for $2T_C = 7$ ms. Both spectra were recorded on a uniformly ^{13}C- and ^{15}N-enriched sample of 7 mg of the BC domain of CNTFR in D_2O, pH 6.3, at 20°C. The lowest contours for spectra (A) and (B) are drawn at the same level and contours are spaced by a factor of 1.20. The spectra were obtained with identical processing parameters using the nmrPipe software package (*16*).

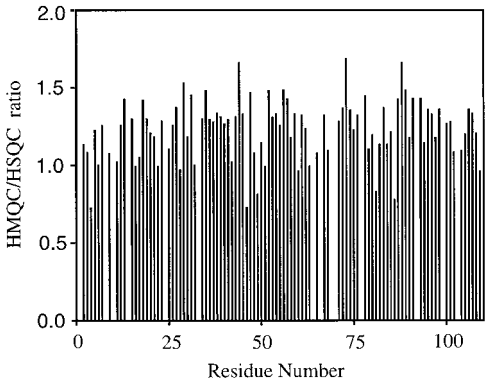

FIG. 3. The ratios of the volumes of the peaks of the 3D HMQC-HCACO spectrum to the corresponding peaks of the 3D HSQC-HCACO spectrum by residue number for $2T_C = 7$ ms.

FID is obtained by subtracting S_{11} from S_{12} and S_{21} from S_{22}, with an additional 90° phase shift being applied (*9–12*). The 3D spectrum can be obtained by using normal Fourier transformation.

To demonstrate the sensitivity enhancement of the HMQC approach over the HSQC method, we applied the HMQC-HCACO and its corresponding HSQC-HCACO experiment, on a Varian Inova 500 MHz NMR spectrometer. A ^{13}C- and ^{15}N-labeled sample of the BC domain of the CNTFR, dissolved in D_2O at 20°C, was used. Figure 2 shows 2D slices from the 3D HMQC-HCACO spectrum (A) and the corresponding 3D HSQC-HCACO spectrum (B), taken at $^{13}C^{\alpha} = 53.85$ ppm, for $2T_C = 7$ ms. Data matrices of 50* × 40* × 512* (* denotes a complex number), in the time domain, were acquired for the two spectra, with spectral widths of 3000, 7000, and 4000 Hz, respectively. The number of transients for each FID was 16. Spectral matrices of 128 × 128 × 512 points for both 3D spectra were obtained with identical processing parameters. Figure 2 clearly indicates that the sensitivity of the HMQC-HCACO experiment is increased considerably when compared with that of HSQC-HCACO experiment. The ratios of the peak volumes of the 3D HMQC-HCACO spectrum to the peak volumes of the corresponding 3D HSQC-HCACO spectrum are shown, by residue number, in Fig. 3. Empty positions in Fig. 3 correspond to residues whose $^1H^{\alpha}$ chemical shift was near the residual solvent peak at 4.7 ppm, as their intensities are difficult to measure precisely. Peaks with ratios smaller than 1 (due to off-resonance spin-lock effects) resonate at $^1H^{\alpha}$ chemical shifts higher than 5.5 ppm. On average, the sensitivity of the 3D HMQC-HCACO spectrum for $2T_C = 7$ ms is enhanced by 23% when compared with the corresponding 3D HSQC-HCACO spectrum.

Figure 4 shows the first 2D planes ($t_2 = 0$) of 3D HMQC-HCACO (A) and HSQC-HCACO (B) experiments for $2T_C = 27$ ms. Data matrices of 128* × 512* points, in the time domain, were acquired for the two spectra, with spectral widths of 3000 and 4000 Hz, respectively. The number of transients for each FID was 32. Spectral matrices of 512 × 1024 points for both 2D spectra were obtained with identical processing parameters. The sensitivity enhancement of the HMQC-HCACO experiment over the HSQC-HCACO experiment exceeds 55%, on average, based on 31 isolated peaks.

By introducing $^1H^{\alpha}$–$^{13}C^{\alpha}$ multiple-quantum coherence into the HCACO experiment we have shown that the sensitivity of this experiment can be increased substantially. This will considerably facilitate the spectral assignment of the backbone atoms of ^{13}C-labeled proteins.

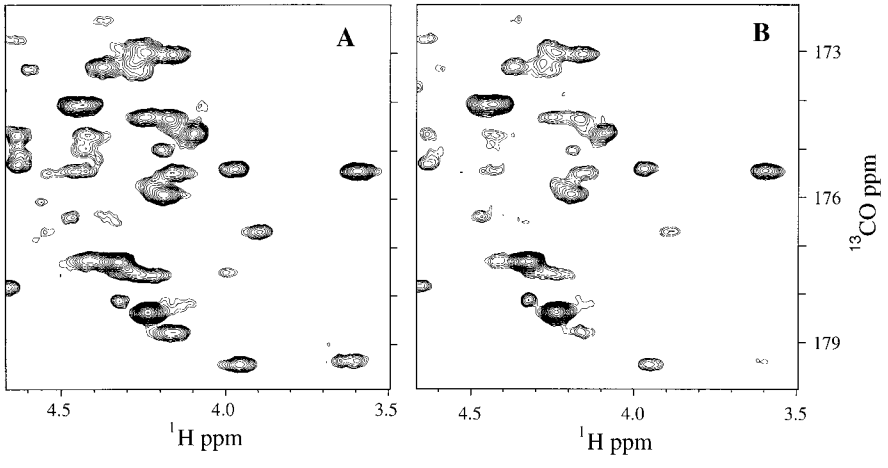

FIG. 4. The first 2D planes ($t_2 = 0$) of the 3D HMQC-HCACO (A) and its corresponding HSQC-HCACO (B) experiment for $2T_C = 27$ ms. The spectra were obtained with identical processing parameters. The lowest contours for spectra (A) and (B) are drawn at the same level and contours are spaced by a factor of 1.20.

ACKNOWLEDGMENTS

This work is supported by grants (HKUST6197/97M and HKUST6038/98M) from the Research Grant Council of Hong Kong. We thank Dr. K. H. Sze for critical discussions. The Hong Kong Biotechnology Research Institute is acknowledged for the purchase of the 500-MHz NMR spectrometer.

REFERENCES

1. L. E. Kay, M. Ikura, R. Tschudin, and A. Bax, *J. Magn. Reson.* **89,** 496–514 (1990).
2. R. Powers, A. M. Gronenborn, G. M. Clore, and A. Bax, *J. Magn. Reson.* **94,** 209–213 (1991).
3. A. G. Palmer, W. J. Fairbrother, J. Cavanagh, P. E. Wright, and M. Rance, *J. Biomol. NMR* **2,** 103–108 (1992).
4. S. Grzesiek and A. Bax, *J. Magn. Reson. B* **102,** 103–106 (1992).
5. R. Bazzo, D. O. Cicero, and G. Barbato, *J. Magn. Reson. B* **107,** 189–191 (1995).
6. F. Lohr and H. Ruterjans, *J. Magn. Reson. B* **109,** 80–87 (1995).
7. R. H. Griffey and A. G. Redfield, *Q. Rev. Biophys.* **19,** 51–82 (1987).
8. S. Grzesiek and A. Bax, *J. Biomol. NMR* **6,** 335–339 (1995).
9. G. Zhu, X. M. Kong, and K. H. Sze, *J. Magn. Reson.* **135,** 232–235 (1998).
10. X. M. Kong, K. H. Sze, and G. Zhu, *J. Biomol. NMR* **14,** 133–140 (1999).
11. A. G. Palmer, J. Cavanagh, P. E. Wright, and M. Rance, *J. Magn. Reson.* **93,** 151–170 (1991).
12. L. E. Kay, P. Keifer, and T. Saarinen, *J. Am. Chem. Soc.* **114,** 10663–10665 (1992).
13. M. Sattler, M. G. Schwendinger, J. Schleucher, and C. Griesinger, *J. Biomol. NMR* **5,** 11–22 (1995).
14. J. Schleucher, M. Schwendinger, M. Sattler, P. Schmidt, O. Schedletzky, S. J. Glaser, O. W. Sorensen, and C. Griesinger, *J. Biomol. NMR* **4,** 301–306 (1994).
15. J. Cavanagh and M. Rance, *Annu. Rep. NMR Spectrosc.* **27,** 1–58 (1993).
16. F. Delaglio, S. Grzesiek, G. Vuister, G. Zhu, J. Pfeifer, and A. Bax, *J. Biomol. NMR* **6,** 277–293 (1995).